ADVANCED OPTICAL MATERIALS
www.advopticalmat.de

Bulk-Size and Highly Transparent Composite Phosphor for NIR Spectroscopy

Liangliang Zhang, Dandan Wang, Feng Liu, Hao Wu, Guohui Pan, Huajun Wu, Zhendong Hao, and Jiahua Zhang**

Near-infrared (NIR) phosphors offer a novel luminescent solution for NIR spectroscopy, but their efficiency remains low. Herein, it is demonstrated that the high transparency of a phosphor improves its external quantum efficiency by developing a new inorganic–organic composite phosphor. The new bulk-size and highly transparent composite phosphor is fabricated through layer-by-layer assembly of micron-sized hexagonal $LiSrAlF_6:Cr^{3+}$ powder phosphor. The inline transparency of the final bulk phosphor can be controlled from 0% to 90.2% at a large solid concentration of ≈47 vol.%. With high transparency, the new bulk phosphor allows the phosphor-conversion light-emitting diode (pc-LED) a 2.9 times improvement in efficiency. This paper inspires a feasible and low energy consumption method to facilitate next-generation NIR pc-LED phosphors.

1. Introduction

Near-infrared (NIR) phosphor-converted light-emitting diodes (pc-LEDs) are smart NIR light sources that can outshine inefficient halogen lamps as a new generation of technology.[1,2] However, their electro-optical efficiency is limited by the low external quantum efficiency (EQE) of the NIR phosphor,[3–5] which has a poorly absorbing luminescence center Cr^{3+} with a cross-section of only 10^{-19}–10^{-20} cm^2.[6,7] Attempts to modify the parity-forbidden nature of Cr^{3+} have not increased the EQE of NIR powder phosphor beyond 50%.[8,9] Recently, transparent bulk phosphors have been shown to achieve much higher EQE (>70%) than opaque powder phosphors,[10–12] owing to their high transparency that allows deeper penetration and better absorption of the excitation light. Currently reported bulk-size NIR phosphors are all-inorganic materials such as transparent ceramics, single crystal, phosphor in glass, and phosphor in ceramics. These all-inorganic phosphors need long-time and high-temperature treatment to consume much energy and are always high cost. Inorganic-organic composites offer a flexible phosphor design method and are easy to fabricate with less energy consumption, gaining advantages over traditional all-inorganic materials.

The composite phosphor (CP) in bulk size is usually made by dispersing inorganic particles in an organic matrix.[13,14] To achieve high transparency, Mie and Rayleigh scattering at the inorganic-organic interface must be minimized. The so-called nanocomposite[15–17] is designed by reducing the inorganic particle size to nanometer scale to minimize scattering. However, the nano-sized particles have low luminous efficiency due to severe surface quenching.[18] Moreover, the solid content of the nanocomposite is limited to 5–15 vol.%,[19,20] which is too low for strong absorption. Micron-sized inorganic particles can solve these problems, but they suffer from strong Mie scattering and birefringence,[21,22] resulting in a "milky" bulk. Birefringence causes light to split into two when passing through an optically anisotropic particle, leading to transparency loss. So far, no method has been developed to design bulk-size and highly transparent CP with micron-size particles and large solid concentrations.

The nacre-like structure, which resembles a "brick-and-mortar-like" arrangement of inorganic flake-shaped particles and organic material,[23] may address the scattering problems mentioned above. The well-aligned flakes avoid birefringence by sharing a global crystallographic direction and are close-packed to achieve a high solid content of up to 95 vol.%.[24] The layer-by-layer structure can extend to 100 mm[25] in thickness to form a bulk-size material. However, most reported nacre-like materials are opaque, with only Magrini[26] reporting a bulk translucent glass and PMMA composite with 2% in-line transparency. Light scattering is mainly caused by the mismatch of refractive index and the presence of pores. For example, polyvinyl butyral (PVB) is a necessary additive in the sedimentation process but has a different refractive index.[27] Eliminating the porosity between

L. Zhang, H. Wu, G. Pan, H. Wu, Z. Hao, J. Zhang
State Key Laboratory of Luminescence and Applications
Changchun Institute of Optics
Fine Mechanics and Physics
Chinese Academy of Sciences
3888 Eastern South Lake Road, Changchun 130033, China
E-mail: zhangliangliang@ciomp.ac.cn; zhangjh@ciomp.ac.cn

D. Wang
Key Laboratory of Functional Materials Physics and Chemistry of the Ministry of Education
Jilin Normal University
Siping 136000, China

F. Liu
Key Laboratory for UV-Emitting Materials and Technology of Ministry of Education
Northeast Normal University
Changchun 130024, China

The ORCID identification number(s) for the author(s) of this article can be found under https://doi.org/10.1002/adom.202301114

DOI: 10.1002/adom.202301114

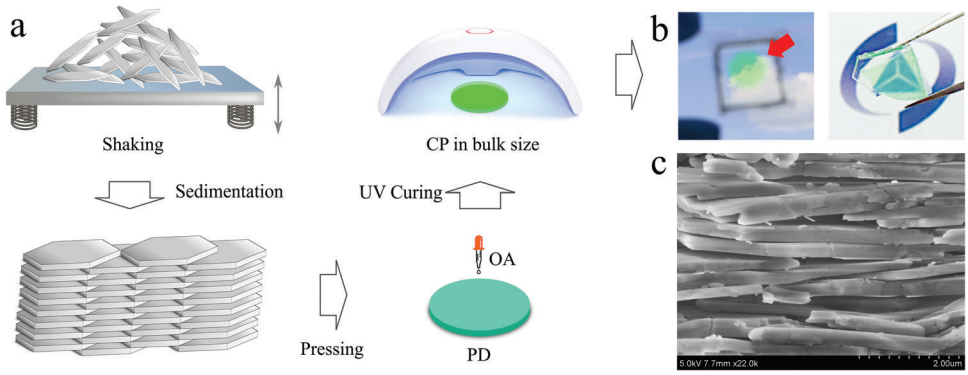

Figure 1. Fabrication of highly transparent $LiSrAlF_6:Cr^{3+}$ CP in bulk size. a) Fabrication process by the sedimentation in air method. b) Photograph of the transparent CP in bulk size. c) SEM image of the nacre-like structure.

polymer and particles is also crucial.[26,28] Although the nacre-like structure is originally developed for tough structural materials, it is also a promising strategy to design highly transparent CP in bulk size.

This paper demonstrates a method to fabricate bulk-size and highly transparent CP consisting of micron-size particles. The CP has in-line transparency of 90.2% and solid content of ≈47 vol.%. The "building block" is $LiSrAlF_6:Cr^{3+}$ powder phosphor with a hexagonal structure to show birefringence.[29,30] New gravitational sedimentation in air method is proposed to construct the nacre-like structure, avoiding incorporating of any additives to mismatch the refractive index. The curing speed of the polymer is also controlled by the exposure intensity to prevent generating new pores. The well-aligned crystalline particles and good refractive index matching are crucial for the highly bulk transparent property.

2. Results and Discussion

2.1. Fabrication Process

The highly transparent CP in bulk size is fabricated by gravitational sedimentation in air method. As shown in **Figure 1**a, $LiSrAlF_6:Cr^{3+}$ powder phosphor with flake-shape particles is put on a shaking system with oscillation in vertical direction. The maximum amplitude is 3 mm with frequency of ≈50 Hz, and the duration only needs 2–5 mins. The flakes are periodically propelled upward off the ground and forced to parallel alignment by air buoyancy as it falls back down. A large aspect ratio of the flake-shaped particle is important because air provides much smaller resistance than liquid. In this paper, the as-prepared flake-shaped $LiSrAlF_6:Cr^{3+}$ powder phosphor has an average aspect ratio of 30–40 with a diameter of 2–13 μm and thickness of 0.2–0.4 μm. The sedimentation produces a pile of loose and unconsolidated powders with a nacre-like structure. Uniaxial pressure with a value of 50 Mpa is applied to consolidate the nacre-like structure. Subsequently, isostatic pressure with 200 Mpa is applied by immersing the bulk body into a liquid medium to get a uniform and dense bulk body with thickness of 0.8 mm and diameter of 10 mm, as shown in Figure 1c. At this end, we realize an opaque phosphor disc (PD) composed of $LiSrAlF_6:Cr^{3+}$ powder phosphor aligned layer by layer. Then, we choose a commercially available liquid optical adhesive (OA, Acrylate resin base) that has a refractive index of ≈1.37 and is curable under UV light to fill the pores inside PD, reaching a solid content of ≈47 vol.% (or ≈85% in mass fraction). The curing rate is controlled by intensity of the UV light with an initial curing energy of less than 0.1 J/cm^2 and an ultimate curing energy >6 J cm^{-2}. Finally, we realize a highly transparent CP in bulk size with micron-sized $LiSrAlF_6:Cr^{3+}$ flakes as building block. As shown in Figure 1b, one can look through the CP to recognize clouds and icons. The fabrication process avoids high-temperature treatment and can quickly get a highly transparent phosphor bulk, showing advantages over traditional all-inorganic routines.

2.2. Optical and Luminescence Property

Figure 2a is the transmittance spectra of CP to show an in-line transparency of 90.2%, which is 96.06% of the theoretical value. The absorption peaks at 433 and 640 nm are ascribed to Cr^{3+} in $LiSrAlF_6$ and OA causes the strong absorption band at wavelength <400 nm. Figure 2b shows the collimated transmission intensity of a 780 nm laser passing through the CP or OA, which moves in a straight line with step of 0.5 mm. The relative intensity of the 780 nm laser passing CP is 95.8%, similar to the calculated 96.06% of theoretical transparency. Residual analysis of these data points shows a residual of transmitted intensity at each step is no more than 1.2% both for the CP and OA, as shown in Figure S2b (Supporting Information), to indicate a good uniformity of CP. Scattering at the interface of CP and OA causes the sudden decrease in intensity at 3.5 mm, which is not included in residual analysis. The luminescence property of CP is almost the same as $LiSrAlF_6:Cr^{3+}$ powder phosphor, as shown in Figure 2c. The $LiSrAlF_6:Cr^{3+}$ powder phosphor has three excitation peaks at 287, 433, and 640 nm, ascribed to $^4T_{1u}$, $^4T_{1g}$, and $^4T_{2g}$ energy levels of Cr^{3+}. The broad NIR emission at 808 nm originates from $^4T_{2g} \rightarrow {}^4A_{2g}$ transition. The excitation and emission peaks of CP overlap with that of $LiSrAlF_6:Cr^{3+}$ powder phosphor, except the excitation peak at 287 nm for the strong absorption of UV light by OA.

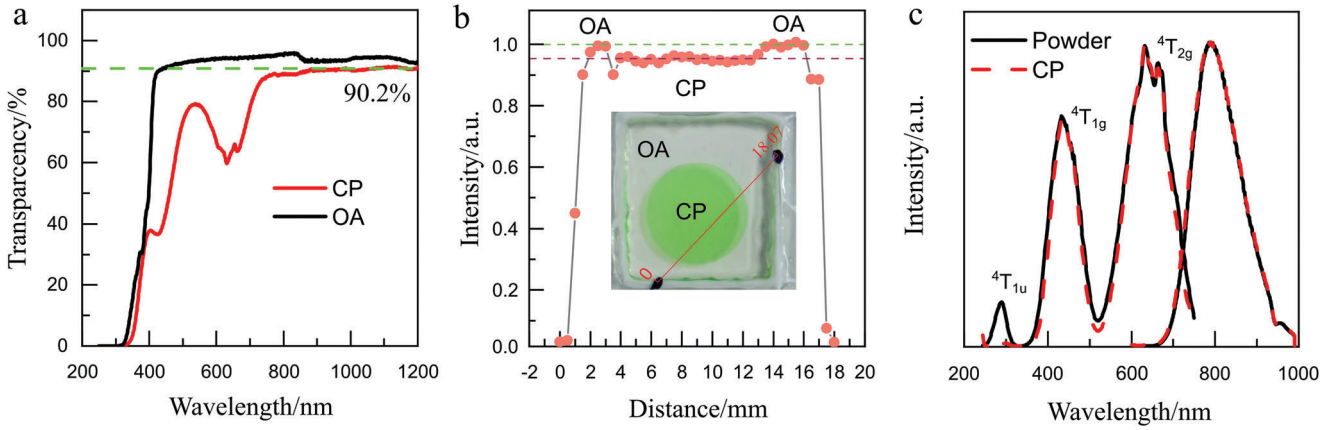

Figure 2. Optical and luminescent property of CP. a) The transmittance spectrum. b) Collimated transmission measurement at different position. The insert photograph shows the move track of the 780 nm laser. c) The excitation and emission spectra.

2.3. Arrange the Crystalline Flakes

When substituting Sr^{2+} by Ca^{2+}, the $LiSrAlF_6:Cr^{3+}$ flakes transform from single-crystal to polycrystal but with refractive index almost unchanged.[31] As shown in **Figure 3**a, $LiSrAlF_6:Cr^{3+}$ flakes are imperfect hexagons in shape with a smooth surface. The electron diffraction pattern in Figure 3b shows spots also arranged in a hexagon shape to indicate a crystalline particle. For comparison, $LiCaAlF_6:Cr^{3+}$ flakes fabricated by the same method show an ideal hexagon shape but with a rough surface, as shown in Figure 3e. The electron diffraction pattern in Figure 3f shows a series of concentric rings to indicate a polycrystal particle. Many spots on the rings may originate from the few gains in one particle that lack enough planes oriented in all directions. Figure 3c is the optical micrograph of $LiSrAlF_6:Cr^{3+}$ taken by incident illumination, illuminating the sample's front surface. One can observe many colorful patterns on the particle surface, which are caused by interference of the light reflected from front and back particle surfaces. Figure 3d is the optical micrograph of $LiSrAlF_6:Cr^{3+}$ taken by transmitted illumination, illuminating the sample's back surface. The particle is observed to be totally transparent. For comparison, the optical micrographs of $LiCaAlF_6:Cr^{3+}$ show a glaring particle under incident illumination and a dark surface with specks of light under transmitted illumination, as shown in Figure 3g,h. These phenomena indicate $LiCaAlF_6:Cr^{3+}$ flake itself is opaque for its polycrystal nature. As a result, CP fabricated by $LiCaAlF_6:Cr^{3+}$ powder phosphor is opaque.

Birefringence is an important scattering routine because $LiSrAlF_6:Cr^{3+}$ has an anisotropic hexagonal lattice. As shown in **Figure 4**a, we disperse $LiSrAlF_6:Cr^{3+}$ powder in 50 wt.% poly acrylic acid (PAA, refractive index ≈1.38) to destroy the nacre-like structure, because PAA is sticky to suspend $LiSrAlF_6:Cr^{3+}$

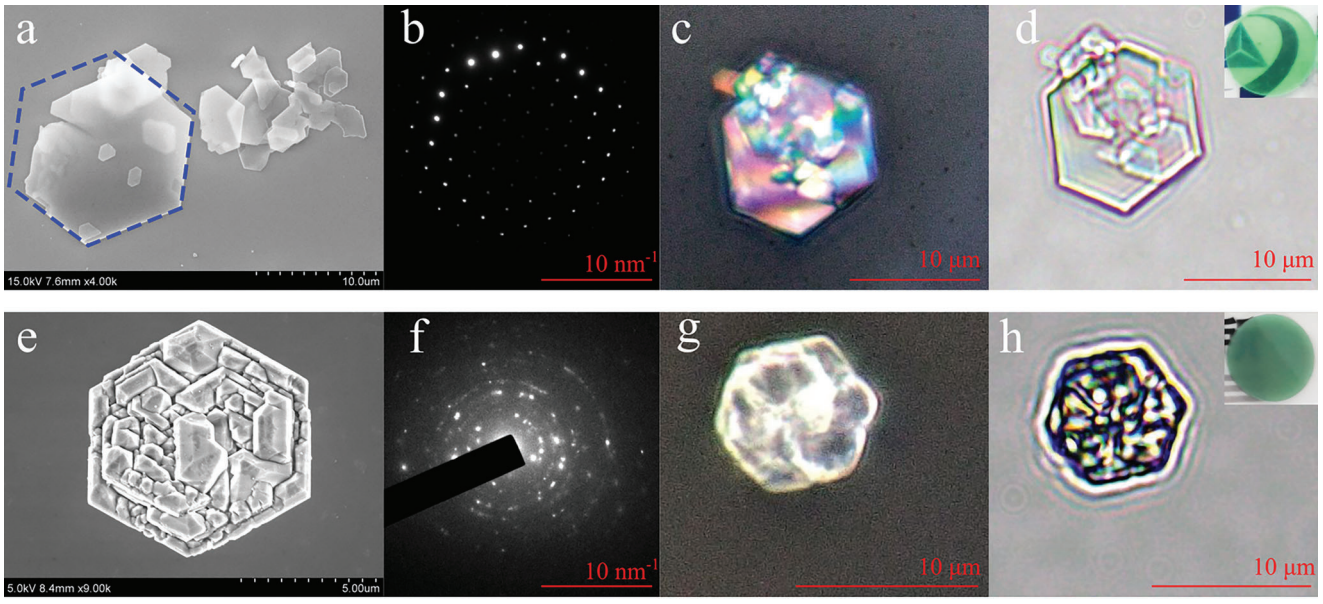

Figure 3. Micrographs of $LiSrAlF_6:Cr^{3+}$ (Top) and $LiCaAlF_6:Cr^{3+}$ (Bottom) flakes. a,e) SEM image. b,f) Electron diffraction pattern. c,g) Optical micrographs under incident illumination. d,h) Optical micrographs under transmitted illumination.

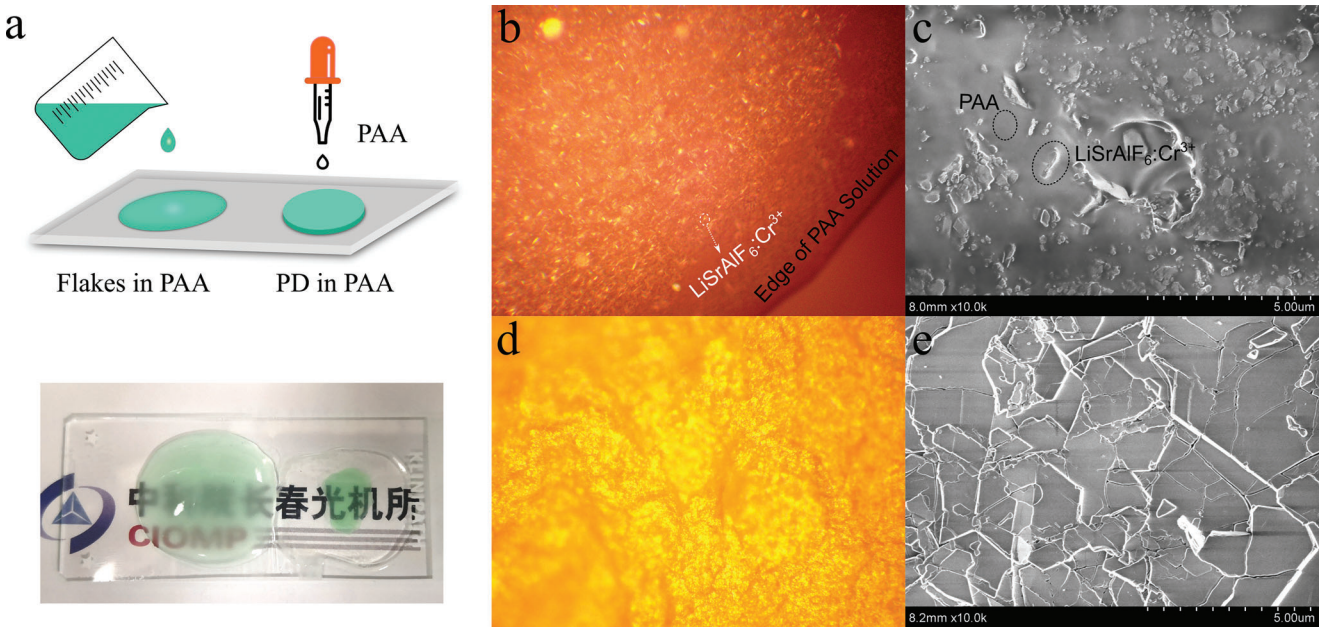

Figure 4. Two methods to align $LiSrAlF_6:Cr^{3+}$ flakes: dispersing powders in PAA and immersing PD in PAA. a) A schematic diagram to show the two methods. b,d) Optical micrograph of powders in PAA (top) and PD in PAA (bottom) under polarized light. c,e) SEM images of powders in PAA (top) and PD in PAA (bottom).

flakes. Under polarized light microscopy, as shown in Figure 4b, we can distinguish the $LiSrAlF_6:Cr^{3+}$ flakes from PAA by their golden body color. The $LiSrAlF_6:Cr^{3+}$ flakes are recognized as elongated dots pointing in various directions and are observed to take random movement inside the PAA solution. The SEM image of the dried mixture also proves a radium distribution of $LiSrAlF_6:Cr^{3+}$ flakes in PAA, as shown in Figure 4c. With the random arrangement of $LiSrAlF_6:Cr^{3+}$ flakes, birefringence loss is dominant to make the whole mixture untransparent, although the refractive index is well matched, as shown in the bottom Figure 4a. For comparison, the well-aligned $LiSrAlF_6:Cr^{3+}$ PD is also immersed in PAA, as shown in Figure 4d,e, to show high transparency. Overall, the nacre-like structure is capable of minimizing birefringence to make the CP highly transparent.

2.4. Refractive Index Match

We choose different organic liquids, such as methyl alcohol, acetone, ethyl alcohol, and isopropyl alcohol, with the reactive index of 1.328, 1.359, 1.362, and 1.375, as pore filler to show the influence of refractive index. As shown in **Figure 5**a, the transparency of PD ranges from translucent to transparent with different immersion liquids. The higher the refractive index of the liquid is, the higher the transparency for a better matching refractive index of $LiSrAlF_6$ (≈1.37). We use the collimated transmission method to determine transparency. As shown in Figure 5c, a 780 nm laser transmits through a quartz container filled with different liquids. The PD is placed on one side of the container while leaving the other empty for calibration. The transparency of PD increases from 38.8% in methyl alcohol to 89.4% in isopropyl alcohol, as shown in Figure 5d.

We can also find a novel change in transparency by controlling the evaporation of a liquid to recycle the PD between opaque and transparent repeatable, as shown in Figure 5a. With the new transparency controllable property, the PD is expected for new applications such as an optical switch or anti-counterfeiting material. The excitation light is hard to arrive at Cr^{3+} inside the opaque PD for scattering, but it can penetrate deep into the bulk to arrive at every Cr^{3+} for the transparent PD. Therefore, the impact of transparency on absorption can be observed in situ by dropping isopropyl alcohol on PD in a diffuse reflection spectrum measurement setup, as shown in Figure 5b. The absorption of Cr^{3+} at 460 nm increases from 24.6% to 77.2%, suggesting the transparent CP can fabricate NIR pc-LED with higher efficiency compared to the opaque one.

2.5. Application

Scattering[32] and reabsorption[33] are the leading light loss routine in a pc-LED package. For the opaque PD with a thickness of 0.8 mm, the reabsorption loss account for ≈6% of total light loss by Gabriela's method,[34] and scattering accounts for ≈72.5%, as shown in **Figure 6**a. As for the transparent CP, reabsorption loss is almost eliminated, and the scattering loss decreases to 22.5%. The internal quantum efficiency (IQE) and external quantum efficiency (EQE) of $LiSrAlF_6:Cr^{3+}$ powder phosphor are measured to be 59.7% and 7.8%, as shown in Figure S7a (Supporting Information). For comparison, the transparent CP in a pc-LED package has a decreased IQE of 46.2% for scattering loss but has a 3.3-time-increased EQE of 26% for better absorption, as shown in Figure S7c (Supporting Information). These phenomena prove that highly transparent property increases the absorption ability of a NIR phosphor to show high EQE.

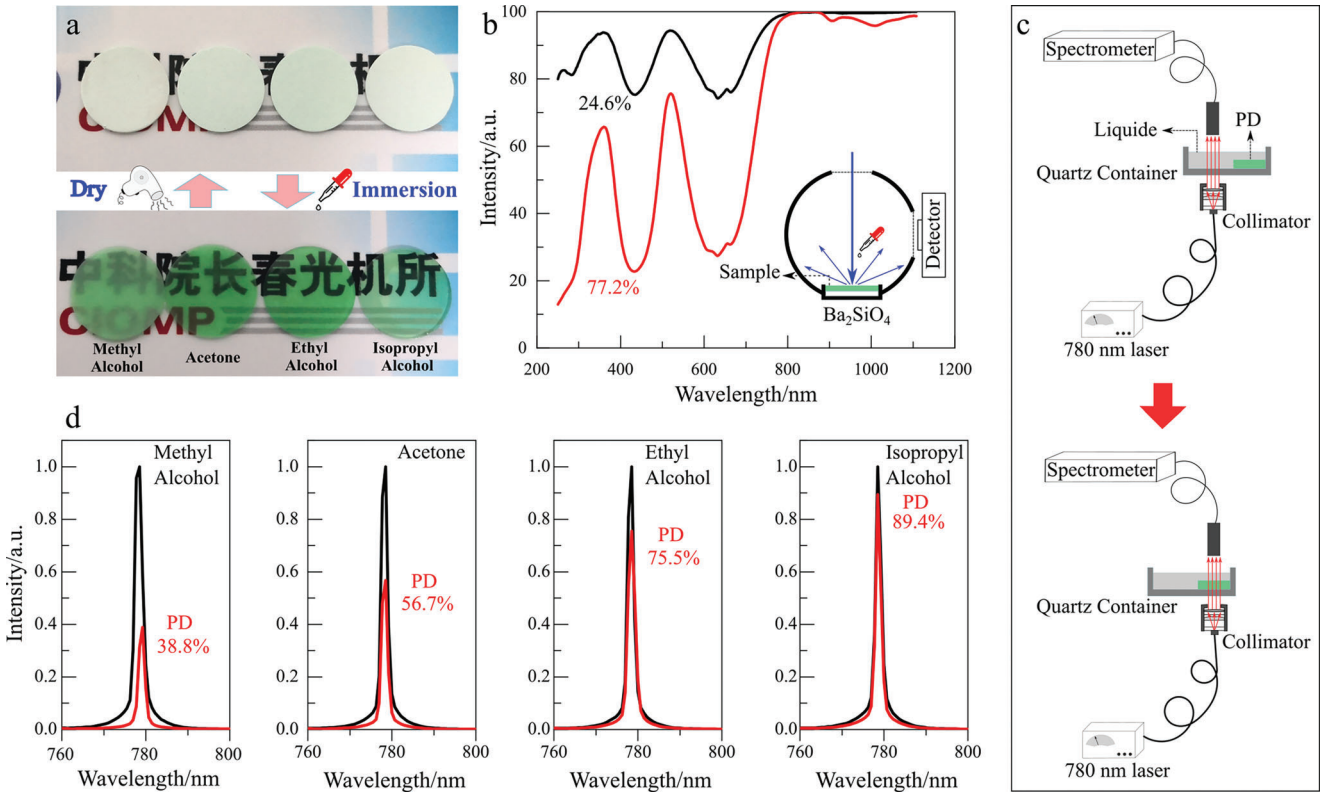

Figure 5. Influence of refractive index on transparency. a) PD immersed in methyl alcohol, acetone, ethyl alcohol, and isopropyl alcohol, respectively. b) Diffuse refection spectra of PD with isopropyl alcohol immersed (red) or not (black). The insert diagram demonstrates the experimental setup inside an integrating sphere. c) Diagram of the collimated transmission method. d) Intensity of the collimated 780 laser transmitted through liquid (black) and PD (red).

The optimized NIR pc-LED is fabricated by 4 mm thick highly transparent CP. The electroluminescence spectra of the optimized NIR pc-LED at different current is shown in Figure 6b. The intensity of the untapped blue light is much weaker than the NIR output to indicate a full use of blue light. For example, the intensity at 450 nm under 100 mA current is 0.09 mW, much <0.3 mW of the NIR light at 810 nm. The peak intensity of 810 nm NIR light increases with the current and reaches the maximum at 200 mA, sacrificing the electro-optical efficiency.

Figure 6c displays the results for the NIR output power and electro-optical efficiency. At a current of 100 mA, the NIR output power is 52.3 mW, and the electro-optical efficiency is 16.8%. When considering different sizes and series-parallel connections of blue LED chips, relying on the electro-optical efficiency at

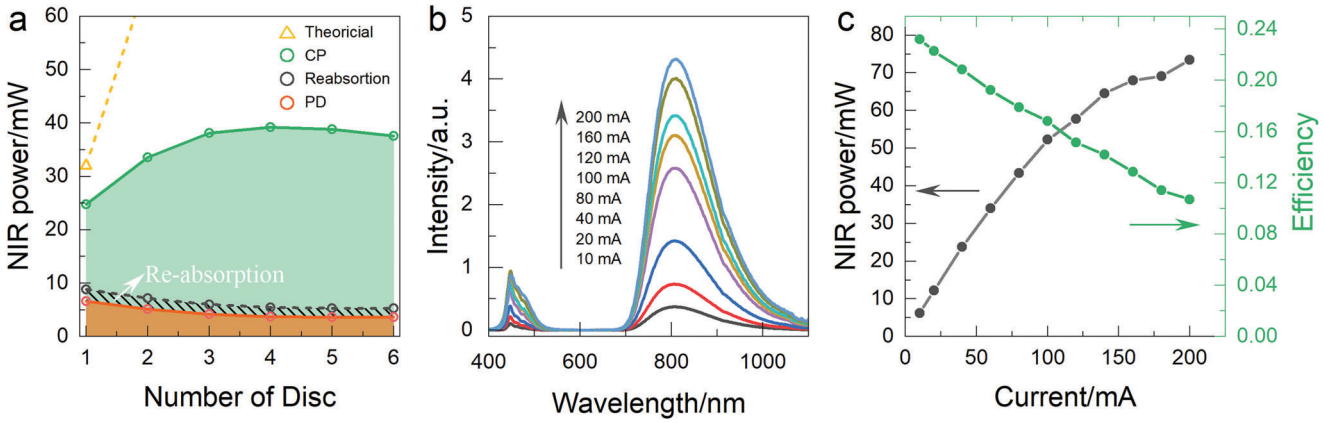

Figure 6. Application in NIR pc-LED. a) NIR output power with different number of PD in thickness of 0.8 mm covered on blue LED chip. b) Electroluminescence spectra of the optimized NIR pc-LED at different current. c) NIR output power and electro-optical efficiency of the optimized NIR pc-LED at different current.

Table 1. NIR pc-LED performance of many typical broadband NIR phosphors.

Materials	NIR output power	$\eta_{pc\text{-}LED}$	Ref.
$Ca_{2-x}Lu_{1+x}Zr_{2-x}Al_{3+x}O_{12}$: Cr^{3+}	9.0 mW @10 mA	33.9% @10 mA	[36]
$Ga_{2-x}In_xO_3$: Cr^{3+}	21 mW @30 mA	26.6% @30 mA	[37]
$LiSrAlF_6$:Cr^{3+} CP	6.32 mW@10 mA	23.2% @10 mA	This work
$LiInSi_2O_6$: Cr^{3+}	51.6 mW @100 mA	23% @10 mA	[38]
$Ca_2LuHf_2Al_3O_{12}$: Cr^{3+}	5.5 mW @10 mA	21.28% @10 mA	[39]
$LiSrAlF_6$:Cr^{3+} powder	11.64 mW @50 mA	8.014% @50 mA	[35]

low current is a more trustworthy indicator than the NIR output power, because it helps avoid the droop effect and makes for a more dependable measurement. In this case, the electro-optical efficiency at 10 mA is 23.2%, among the best-reported materials, as shown in **Table 1**. It's important to note that $LiSrAlF_6$:Cr^{3+} previously had the best-reported electro-optical efficiency of only ≈8%.[35] However, the highly transparent property of $LiSrAlF_6$:Cr^{3+} CP leads to a remarkable 2.9 times improvement in efficiency.

3. Conclusion

In this paper, we show a simple method to make bulk-size and highly transparent inorganic-organic composite phosphor with micron-size particles. We use a gravitational sedimentation in air method to stack the micron-sized $LiSrAlF_6$:Cr^{3+} powder phosphor layer by layer. Even a slight scattering at each flake can make the whole bulk opaque, with ≈2000–4000 flakes across the thickness. We discuss three parameters: 1) Each inorganic particle should be crystalline because a polycrystalline particle itself is not transparent; 2) The nacre-like structure can avoid birefringence loss; 3) A slight change of refractive index from 1.375 to 1.328 reduces transparency from 89.4% to 38.8%. The high bulk transparency can increase the blue light absorption from 24.6% to 77.2% and increase the NIR output power of pc-LED by 7.9 times from 6.6 to 52.3 mW. The transparent composite phosphor in bulk size is a new attempt for the next-generation NIR pc-LED.

Unlike traditional composites with inorganic dopant and organic matrix, the composite phosphor here has inorganic framework and organic pore filler. Filling pores with different organics leads to various new features. As we show in this paper, with a curable optical adhesive as pore filler, we achieve the highly transparent composite phosphor. With vaporizable liquid as pore filler, we achieve a composite that can switch between opaque and transparent for optical applications. Therefore, we expect the composite phosphor with nacre-like structure to inspire a broader application prospect, such as laser gain medium and scintillator.

4. Experimental Section

Preparation of $LiSrAlF_6$:Cr^{3+} Flakes: $LiSrAlF_6$:Cr^{3+} flakes were synthesized by hydrothermal method. Stoichiometric ratio of Li_2CO_3, $Sr(NO_3)_2$, $Al(NO_3)_3{\cdot}9H_2O$, and $Cr(NO_3)_3{\cdot}9H_2O$ were dissolved in deionized water. HNO_3 was added to the mixture under magnetic stirring until forming a clear solution. Then, NH_4F solution was added slowly under magnetic stirring. A mass of white precipitate formed immediately, resulting in a suspension liquid with pH of 2–3. The suspension liquid was transferred into a reactor and was kept at 340 °C for 2 h. The $LiSrAlF_6$:Cr^{3+} flakes were synthesized after centrifuge, washing, and drying.

Preparation of $LiSrAlF_6$:Cr^{3+} Composite: $LiSrAlF_6$:Cr^{3+} powder phosphor was transferred into a steel mold with a diameter of 10 mm. Then, the mold was put on a shaking system with oscillation in the vertical direction. After 2–5 min oscillation, the mold was put in a tablet press for molding. The green body was sealed in a plastic bag then treated with cold isostatic pressure for better strength. A commercially available liquid optical adhesive with a refractive index of ≈1.37 was dripped on the green body. The composite was cured under 400 nm UV light.

Characterization: The excitation spectrum was measured by FL910 spectrometer (Edinburgh Instruments) with a 400 W Xe lamp. The emission spectrum was measured by a microfiber spectrometer (QEPro, Ocean Optics, 200–1000 nm). The diffuse reflection spectra were measured by a UV–vis–NIR spectrometer (UV-3600plus, Shimadzu, Japan) equipped with an integrating sphere. The transparence spectra were also measured by UV-3600plus in a transmission mode. The photomicrograph was taken under Olympus BX53M optical microscope. The temperature-dependent property was measured in a cooling–heating platform (THMS600E, Linkam Scientific Instruments). The SEM image was measured by emission scanning electron microscopy (FE-SEM, Hitachi, S-4800). The electron diffraction pattern was measured by transmission electron microscopy (JEOL-2100) with an accelerating voltage of 200 kV. The photoelectric property of the pc-LED was measured by a photoelectric measuring system (HAAS 2000, 350–1100 nm, EVERFINE).

Supporting Information

Supporting Information is available from the Wiley Online Library or from the author.

Acknowledgements

This work was financially supported by the National Natural Science Foundation of China (grant no. 12074373 and 52072361), the Key Research and Development Program of Jilin province (grant no. 20210201024GX), the Major Science and Technology Project of Anhui Province (2021e03020007), the Changchun science and technology planning project (grant no. 21ZGY05), the Youth Innovation Promotion Association CAS (no. 2020222), and the Opening Project of Key Laboratory of Transparent Opto-functional Inorganic Materials, Chinese Academy of Science.

Conflict of Interest

The authors declare no conflict of interest.

Data Availability Statement

The data that support the findings of this study are available from the corresponding author upon reasonable request.

Keywords

inorganic–organic composites, LED, NIR, phosphors, transparencies

Received: June 25, 2023
Published online: August 17, 2023

[1] M. H. Fang, Z. Bao, W. T. Huang, L. RS, *Chem. Rev.* **2022**, *26*, 1037.
[2] Z. Jia, C. Yuan, Y. Liu, X.-J. Wang, P. Sun, L. Wang, H. Jiang, J. Jiang, *Light: Sci. Appl.* **2020**, *9*, 86.

[3] C. Yuan, R. Li, Y. Liu, L. Zhang, J. Zhang, G. Leniec, P. Sun, Z. Liu, Z. Luo, R. Dong, J. Jiang, *Laser Photonics Rev.* **2021**, *15*, 2100227.
[4] E. Song, H. Ming, Y. Zhou, F. He, J. Wu, Z. Xia, Q. Zhang, *Laser Photonics Rev.* **2021**, *15*, 2000410.
[5] J. Qiao, S. Zhang, X. Zhou, W. Chen, R. Gautier, Z. Xia, *Adv. Mater.* **2022**, *34*, 2201887.
[6] J. Zhong, C. Li, W. Zhao, S. You, J. Brgoch, *Chem. Mater.* **2021**, *34*, 337.
[7] H. Xiao, J. Zhang, L. Zhang, H. Wu, H. Wu, G. Pan, F. Liu, J. Zhang, *Adv. Opt. Mater.* **2021**, *9*, 2101134.
[8] L. Lou, S. Zhao, S. Yuan, D. Zhu, F. Wu, Z. Mu, *Inorg. Chem. Front.* **2022**,*9*, 3522.
[9] M. Shi, L. Yao, J. Xu, C. Liang, Y. Dong, Q. Shao, *J. Am. Ceram. Soc.* **2021**, *104*, 3279.
[10] H. Jiang, L. Chen, G. Zheng, Z. Luo, X. Wu, Z. Liu, R. Li, Y. Liu, P. Sun, J. Jiang, *Adv. Opt. Mater.* **2022**, *47*, 2102741.
[11] G. Zheng, W. Xiao, H. Wu, J. Wu, X. Liu, J. Qiu, *Laser Photonics Rev.* **2021**, *15*, 2100060.
[12] G. Zheng, W. Xiao, J. Wu, X. Liu, H. Masai, J. Qiu, *Adv. Sci.* **2022**, *9*, 2105713.
[13] B. M. Novak, *Adv. Mater.* **1993**, *5*, 422.
[14] J. Loste, J.-M. Lopez-Cuesta, L. Billon, H. Garay, M. Save, *Prog. Polym. Sci.* **2019**, *89*, 133.
[15] A. Dang, S. Ojha, C. M. Hui, C. Mahoney, K. Matyjaszewski, M. R. Bockstaller, *Langmuir* **2014**, *30*, 14434.
[16] Y.-Q. Li, Y. Yang, S.-Y. Fu, X.-Y. Yi, L.-C. Wang, H-Da Chen, *J. Phys. Chem. C* **2008**, *112*, 18616.
[17] Y. Yang, Y.-Q. Li, S.-Y. Fu, H.-M. Xiao, *J. Phys. Chem. C* **2008**, *112*, 10553.
[18] Zi-P Zhang, X. Liu, X. Liu, Z.-W. Lu, X. Sui, Bo-Yu Zhen, Z. Lin, L. Chen, Li-M Wu, *Chem. Mater.* **2022**, *4*, 1976.
[19] R. Chai, H. Lian, Z. Hou, C. Zhang, C. Peng, J. Lin, *J. Phys. Chem. C* **2010**, *114*, 610.
[20] S. Li, M. S. Toprak, Y. S. Jo, J. Dobson, D. K. Kim, M. Muhammed, *Adv. Mater.* **2007**, *19*, 4347.
[21] J. Akiyama, Y. Sato, T. Taira, *Appl. Phys. Express* **2011**, *4*, 022703.
[22] S. M. Antao, *Powder Diffr.* **2013**, *28*, 281.
[23] N. Almqvist, N. H. Thomson, B. L. Smith, G. D. Stucky, D. E. Morse, P. K. Hansma, *Mater. Sci. Eng., C* **1999**, *7*, 37.
[24] O. Oner Ekiz, A. F. Dericioglu, H. Kakisawa, *Mater. Sci. Eng., C* **2009**, *29*, 2050.
[25] M. Mirkhalaf, H. Zreiqat, *JOM* **2020**, *72*, 1458.
[26] T. Magrini, F. Bouville, A. Lauria, H. Le Ferrand, T. P. Niebel, A. R. Studart, *Nat. Commun.* **2019**, *10*, 2794.
[27] S. Behr, U. Vainio, M. Müller, A. Schreyer, G. A. Schneider, *Sci. Rep.* **2015**, *5*, 9984.
[28] T. Magrini, S. Moser, M. Fellner, A. Lauria, F. Bouville, A. R. Studart, *Adv. Funct. Mater.* **2020**, *30*, 2002149.
[29] S. A. Payne, L. L. Chase, L. K. Smith, W. L. Kway, H. W. Newkirk, *J. Appl. Phys.* **1989**, *66*, 1051.
[30] S. A. Payne, L. L. Chase, G. D. Wilke, *J. Lumin.* **1989**, *44*, 167.
[31] T. A. Samtleben, J. Hulliger, *Opt. Lasers Eng.* **2005**, *43*, 251.
[32] S. C. Allen, A. J. Steckl, *Appl. Phys. Lett.* **2008**, *92*, 143309.
[33] M. G Lagorio, E. San Román, *J. Chem. Educ.* **2002**, *79*, 1362.
[34] M. L. Gabriela, S. R. Enrique, *J. Chem. Educ.* **2002**, *79*, 1362.
[35] Di Wu, L. Liu, H. Liang, H. Duan, W. Nie, J. Wang, J. Peng, X. Ye, *Ceram. Int.* **2022**, *1*, 387.
[36] J. Zhang, L. Zhang, F. Liu, H. Wu, H. Wu, G. Pan, Y. Luo, Z. Hao, J. Zhang, *Laser Photonics Rev.* **2022**, 2200586.
[37] J. Zhong, Ya Zhuo, Fu Du, H. Zhang, W. Zhao, J. Brgoch, *ACS Appl. Mater. Interfaces* **2021**, *13*, 27.
[38] X. Xu, Q. Shao, L. Yao, Y. Dong, J. Jiang, *Chem. Eng. J.* **2020**, *383*, 123108.
[39] S. He, L. Zhang, H. Wu, H. Wu, G. Pan, Z. Hao, X. Zhang, L. Zhang, H. Zhang, J. Zhang, *Adv. Opt. Mater.* **2020**, *8*, 1901684.